Fluorescence Lifetimes and Spectra of RPE and Sub-RPE Deposits in Histology of Control and AMD Eyes

Rowena Schultz,[1] Kushmali C. L. K. Gamage,[1] Jeffrey D. Messinger,[2] Christine A. Curcio,[2] and Martin Hammer[1,3]

[1]Department of Ophthalmology, University Hospital Jena, Jena, Germany
[2]Department of Ophthalmology and Visual Sciences, School of medicine, University of Alabama at Birmingham, Birmingham, Alabama, United States
[3]Center for Medical Optics and Photonics, University of Jena, Jena, Germany

Correspondence: Rowena Schultz, University Hospital Jena, Department of Ophthalmology, Am Klinikum 1, 07747 Jena, Germany; rowena.schultz@med.uni-jena.de.

Received: May 1, 2020
Accepted: August 16, 2020
Published: September 8, 2020

Citation: Schultz R, Gamage KCLK, Messinger JD, Curcio CA, Hammer M. Fluorescence lifetimes and spectra of RPE and Sub-RPE deposits in histology of control and AMD eyes. *Invest Ophthalmol Vis Sci.* 2020;61(11):9. https://doi.org/10.1167/iovs.61.11.9

Purpose. To investigate fluorescence lifetimes as well as spectral characteristics of drusen and RPE autofluorescence in AMD.

Methods. Fluorescence lifetimes and spectra of five eyes with AMD and nine control eyes were analyzed in cryosections by means of two-photon excited fluorescence at 960 nm. Spectra were detected at 490 to 647 nm. Lifetimes were measured using time-correlated single photon counting in two spectral channels: 500 to 550 nm and 550 to 700 nm. Fluorescence decays over time were approximated by a series of three exponential functions. The amplitude-weighted mean fluorescence lifetime was determined.

Results. We identified 196 sub-RPE deposits (AMD, $n = 76$; control, $n = 120$) and recorded 241 RPE sites. The peak emission wavelength of sub-RPE deposits was significantly green shifted compared with RPE (peak at 570 nm vs. 610 nm), but did not differ between AMD and control donors. Sub-RPE deposits showed considerably longer mean fluorescence lifetimes than RPE (ch1, 581 ± 163 ps vs. 177 ± 25 ps; ch2, 541 ± 125 ps vs. 285 ± 31 ps; $P < 0.001$). Sub-RPE deposits found in AMD eyes had longer lifetimes than deposits of controls (ch1, 650 ± 167 ps vs. 537 ± 145 ps; ch2, 600 ± 125 ps vs. 504 ± 111 ps; $P < 0.001$). In AMD eyes, sub-RPE deposits showed a more homogenous autofluorescence distribution and more deposits were larger than 63 µm than in control eyes.

Conclusions. Ex vivo fluorescence imaging of sub-RPE deposits in cross-sections enables the separation of their autofluorescence from that of over- or underlying structures. Our analysis showed considerable variability of sub-RPE deposit lifetimes but not spectra. This indicates that sub-RPE deposits either consist of a variety of different fluorophores or expose the same fluorophores to different microenvironments.

Keywords: age-related macular degeneration, retinal pigment epithelium, drusen, fundus autofluorescence, fluorescence lifetime, fluorescence spectra

Although clinical fundus autofluorescence imaging (FAF) is a routine investigation technique in ophthalmology, especially in the diagnostics of AMD, the origin of the fluorescence signal is not fully understood yet. Different patterns of FAF are described and, in part, related to drusen and hyperpigmentation.[1,2] In vivo, different fluorescence lifetime and spectral characteristics of RPE, RPE detachments, sub-RPE deposits, and drusen were revealed by fluorescence lifetime imaging ophthalmoscopy (FLIO).[3–6] Drusen show a variety of lifetimes[6]. Additionally, this clinical FLIO investigation showed spectral differences between the autofluorescence emission of drusen and surrounding retina/RPE.[6] This differences in lifetime and spectra may reflect different chemical composition. Whereas dominating fluorophores in the RPE are retinal-derived compounds,[7,8] drusen/sub-RPE deposits contain considerable fractions of lipids, phospholipids, (lipo-)proteins, and minerals.[9]

Because FAF as well as FLIO provide en face images with no depth resolution, autofluorescence from various fundus layers is summed up in these signals. This overlay of diverse fluorophores from different anatomic structures makes it difficult to differentiate and characterize them. Thus, insight can be gained by complementing in vivo observations by histology. Marmorstein et al.[10] investigated autofluorescence emission spectra of RPE, sub-RPE deposits, and Bruch's membrane upon excitation at different wavelengths. These authors reported shorter peak emission wavelengths for sub-RPE deposits than for lipofuscin in RPE cells. Additionally, recent en face ex vivo imaging revealed different spectra for drusen and RPE.[11] Measurements of histologic fluorescence lifetimes, as opposed to spectra, are limited to two eyes reported by Schweitzer et al.,[12] who found considerably longer lifetimes in drusen than in RPE.

Therefore, in this study we measured autofluorescence spectra and lifetimes on 196 sub-RPE deposits (without

Investigative Ophthalmology & Visual Science

differentiating periphery and macular regions owing to limited material available) and 241 sites in RPE to check for differences between AMD and control eyes as well as small and larger sub-RPE deposits. This information could give hints on autofluorescence characteristics pointing to the development or progression of AMD.

Methods

Human Donor Tissue

The use of human tissues was approved by institutional review at UAB (#N170213002). Donor eyes were obtained (by author CAC) from Advancing Sight Network (formerly the Alabama Eye Bank) for the purpose of independent studies that compared spectral and molecular characteristics of tissues processed fresh and paraformaldehyde fixed from the same donor.[13] Eyes of Caucasian donors aged 80 years or older without diabetes mellitus and lacking a history (from the medical record or family report) of head traumata, surgeries affecting the retina, or conditions other than AMD affecting the macula (macular edema, macular hole, retinitis pigmentosa), were collected within 6 hours of death and processed immediately. Before processing for histology, all eyes were opened anteriorly and subjected to an expert examination (by author CAC) including post mortem fundus inspection, ex vivo color fundus photography, and ex vivo optical coherence tomography (Spectralis, Heidelberg Engineering, Heidelberg, Germany).

To determine the effect of fixation on autofluorescence, two eyes from each donor were embedded together so that a tissue section from each eye was present on the same glass slide for subsequent analysis. From each donor eye, the cornea and a 2-mm wide scleral rim was removed. For the left eye, the iris and lens were removed, the fundus photographed internally, then the tissue placed directly into carboxymethylcellulose (C9481 Sigma Aldrich, St. Louis, MO) for freezing at –80°C. The right eye was preserved in 4% paraformaldehyde in 0.1 M phosphate buffer for at least 24 hours before iris and lens removal, imaging, embedding in carboxymethylcellulose next to the frozen left eye, and freezing at –80°C. Before freezing, the posterior poles of both eyes were trimmed to 14-mm wide belts of retina, choroid, and sclera containing major landmarks (optic nerve head, fovea, and horizontal meridian of the visuotopic map) and extending anteriorly to pigmented tissue (ora serrata) at the edge of the ciliary body. For diagnostic purposes, serial 12-µm cryosections were collected starting at the superior edge of the optic nerve head (of the preserved eyes). Sections were captured on prelabeled 1 × 3 mm glass slides coated with 10% poly-L-lysine (Sigma Aldrich) and warmed to 37°C. To verify diagnosis and identify pathologic features of interest, every 20th slide was stained with periodic acid-Schiff hematoxylin (K047 kit, Poly Scientific RD, Bayshore, NY) to show basal laminar deposit, lipofuscin, and cell nuclei. Following histology and fundus post mortem inspections, eyes were graded as unremarkable (with only small or infrequent deposits and RPE changes and normal maculae) or AMD, if they had obvious deposits, RPE damage, or changes in the macula region.

Nearby unstained slides were shipped by overnight courier to Jena for fluorescence lifetime microscopy (3–4 slides per eye). The paired eyes of nine donors (mean age, 84.3 ± 3.4 years) were used in this study.

Spectral and Fluorescence Lifetime Imaging

Autofluorescence spectra and lifetimes were recorded using an inverted multiphoton laser scanning microscope (Axio Observer Z.1 and LSM 710 NLO, 63× oil immersion objective [Plan-Apochromat NA = 1.4]; Carl Zeiss, Jena, Germany) in combination with a femtosecond Ti:Sapphire laser (Chameleon Ultra, Coherent Inc., Santa Clara, CA) and a single photon counting fluorescence lifetime imaging setup (Becker & Hickl GmbH, Berlin, Germany). The Ti:Sapphire laser has a pulse repetition rate of 80 MHz with a pulse duration of 140 fs. The excitation wavelength for spectral and lifetime recordings was set to 960 nm.

The spectral QUASAR detector of the LSM710 has been used for spectral imaging. Backscattered excitation light was blocked by a beam splitter selecting the wavelength range of 405 to 710 nm and the fluorescence emission was recorded in the range of 490 to 674 nm with a spectral resolution of 9.6 nm. All spectral images were recorded as an average of 40 fast scans (pixel dwell time of 1.6 µs) with a resolution of 512 × 512 pixel and a field of view of 96.4 × 96.4 µm.

The lifetime imaging measurements are based on the principle of time-correlated single photon counting. A single photon counting setup, consisting of two hybrid photomultiplier tubes (HPM-100-40) in nondescanned operation, each in combination with a SPC-150 time-correlated single photon counting board, was used. Other components included are an optical beam splitter (LP555/BP500-550) to measure two-photon-excited fluorescence in two spectral channels (short spectral channel [SSC] 500–550 nm and long spectral channel [LSC] 550–700 nm). The excitation wavelength (960 nm) was cut off by a filter BG 39 (Schott, Mainz, Germany). All fluorescence lifetime imaging microscopy (FLIM) images have been acquired as an average of 90 fast scans (mean photon count per pixel of approximately 1000; pixel dwell time of 3.1 µs) with a resolution of 256 × 256 pixel and a field of view of 96.4 × 96.4 µm.

The fluorescence decay images from the FLIM detectors were analyzed using the software SPCImage 7.4 (Becker & Hickl GmbH, Berlin, Germany), which is described in detail elsewhere.[14] For decay data fitting, a 3 × 3 pixel binning was applied. The decays where approximated with a three-exponential model yielding in three decay time constants and three amplitudes. For further analysis, the intensity-weighted mean value of the time constants was calculated, denoted here as the mean fluorescence lifetime.

For each FLIM recording, regions of interests (the ROIs are the sub-RPE deposits and RPE near the deposit) were selected in SPCImage, and the averaged mean fluorescence lifetimes per ROI was used for further analysis. Sub-RPE deposits were categorized according to their size and appearance in autofluorescence intensity images (graded by authors RS and KCLKG). Differences in homogeneity and shape were taken into account. Localization of the deposits (macular or periphery) was not considered. Homogenous sub-RPE deposits showed an even distribution of autofluorescence signal with low variability. Nonhomogenous sub-RPE deposits displayed many small internal patches of different fluorescence intensities. The sub-RPE deposits shape was either convex with a round silhouette and clear defined outlines to the overlaying RPE, or irregular with undefined contours and partially no clear separation to the RPE.

For each spectral image, ROIs were selected in the software ZEN black 2.3 (Carl Zeiss Microscopy GmbH, Jena, Germany) and the average spectrum per ROI was used for

Investigative Ophthalmology & Visual Science

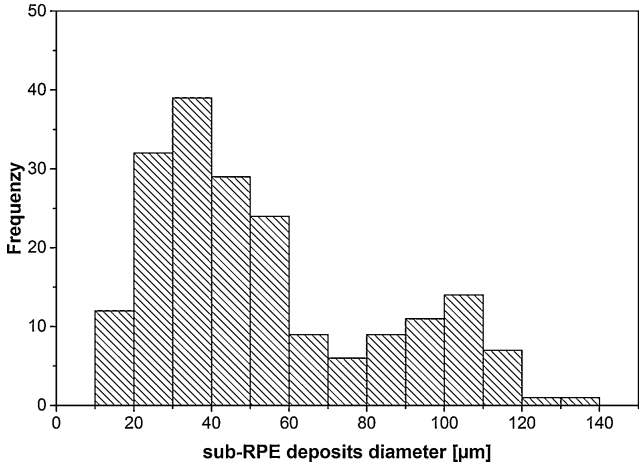

Figure 1. Histogram of sub-RPE deposit size.

further analysis. For comparison of spectra between RPE and sub-RPE deposits in control and AMD eyes, spectra were normalized to 1 by peak normalization (division of all values by maximum intensity value). For intensity analysis, the area under the curve of recordings with both RPE and sub-RPE deposits where used and a quotient of RPE/sub-RPE deposits per image calculated. Sub-RPE deposit diameter was measured as a cross-sectional length along Bruch's membrane.

Statistical analysis was performed using SPSS 26 (IBM, SPSS Inc., Chicago, IL). Distribution and size of sub-RPE deposits between control and AMD donor eyes was tested by the χ^2 test. Group mean values of lifetimes were compared by an unpaired t test. Differences of spectra between fixed and unfixed tissue, RPE and sub-RPE deposits, and sub-RPE deposit size, as well as diagnosis were analyzed by fitting a quadratic polynomial mixed model with spectra and category (RPE vs. sub-RPE deposits, small vs. large sub-RPE deposits, or AMD vs. control) as fixed effects and random intercept. To estimate the differences, an interaction of spectra and category as well as spectra squared and category is included in the model. For correlation exploration between RPE and sub-RPE deposits for intensity and lifetimes, Pearson's r was calculated.

Results

Sub-RPE Deposit Categories

Overall, 196 sub-RPE deposits were found in 15 of 18 donor eyes. Four eyes were diagnosed with AMD by post mortem expert fundus inspection and optical coherence tomography followed by histology. More sub-RPE deposits were found over the whole section (macular and periphery) in AMD eyes: 76 sub-RPE deposits in 4 eyes (19 ± 9 sub-RPE deposits per eye) vs. 120 sub-RPE deposits in 11 of 14 control eyes (9 ± 11 sub-RPE deposits per eye). The diameter of the sub-RPE deposits showed a bimodal distribution (Fig. 1). Thus, in accordance with clinical diagnostic criteria, we distinguished between small sub-RPE deposits (n = 140) with a diameter of less than 63 µm and sub-RPE deposits larger than 63 µm in diameter (n = 56). AMD eyes had more sub-RPE deposits of greater than 63 µm than controls (AMD, 34/76 sub-RPE deposits [44.7%] vs. controls, 22/120 sub-RPE deposits [18.3%]; χ^2 = 15.9; P < 0.001).

Table 1. Mean Fluorescence Lifetimes (τ_m) for RPE and Sub-RPE Deposits in Fresh Frozen and Fixed Tissue

	Fresh Frozen	Fixed	*P* Value
RPE SSC	176 ± 22	178 ± 28	0.467
RPE LSC	289 ± 27	283 ± 35	0.154
Sub-RPE deposits SSC	572 ± 140	589 ± 184	0.46
Sub-RPE deposits LSC	540 ± 110	542 ± 139	0.91

Values are mean ± standard deviation. fresh frozen samples N = 117 for RPE and 98 for sub-RPE deposits, fixed samples n = 124 for RPE and 98 for sub-RPE deposits, results for the short- (SSC) and long-wavelength spectral channel (LSC) are given, statistic by unpaired Student t test.

Table 2. Mean Fluorescence Lifetimes (τ_m) for RPE and Sub-RPE Deposits in Control and AMD Donor Eyes

	Control	AMD	*P* Value
RPE SSC	169 ± 23	195 ± 19	<0.001
RPE LCS	275 ± 27	308 ± 27	<0.001
Sub-RPE deposits SSC	537 ± 145	650 ± 167	<0.001
Sub-RPE deposits LSC	504 ± 111	600 ± 125	<0.001

Values are mean ± standard deviation. Control n = 164 for RPE and 120 for sub-RPE deposits, AMD n = 77 for RPE and 76 for sub-RPE deposits, results for the short- (SSC) and long-wavelength spectral channel (LSC) are given, statistic by unpaired Student t test.

We further distinguished the following categories of sub-RPE deposits according to their appearance in fluorescence intensity images: homogenous content (75/196 sub-RPE deposits [38.3%]; Figs. 2A, 2B), nonhomogenous content (121/196 sub-RPE deposits [61.7%]; χ^2 = 65.9; P < 0.001, Figs. 2C, 2D), convex shape (86/196 sub-RPE deposits [43.9%]; Figs. 2A, 2C), irregular shape (110/196 sub-RPE deposits [56.1%]; Figs. 2B, 2D). Figure 2 also shows autofluorescence of Bruch's membrane, which we did not quantify, because measurements of this thin structure would have been greatly influenced by neighboring RPE, sub-RPE deposits, and choriocapillaris.

Fluorescence Lifetimes

First we checked for the influence of tissue fixation on the fluorescence lifetimes. Because these values did not significantly differ either for RPE or for sub-RPE deposits (Table 1), we did not distinguish between fresh frozen samples and those that were preserved in paraformaldehyde before deep freezing and slicing.

To evaluate the variability of measurements, we determined the coefficient of variation for lifetimes within one eye and calculated the mean over all 18 eyes. For RPE the mean coefficient of variation was 0.11 ± 0.04 (SSC) and 0.08 ± 0.03 (LSC) and for sub-RPE deposits 0.22 ± 0.08 (SSC) and 0.16 ± 0.05 (LSC). For further analysis, no subdivision into single eyes was made. All data were grouped for control eyes (n = 14) and AMD eyes (n = 4).

Sub-RPE deposits showed longer lifetimes (SSC, 581 ± 163 ps; LSC, 541 ± 125 ps; n = 196) than RPE (SSC, 177 ± 25 ps; LSC, 285 ± 31 ps; n = 230). These differences were highly significant (P < 0.001) for both spectral channels. Whereas RPE fluorescence lifetimes were relatively homogeneous, sub-RPE deposits lifetimes showed a high variability (Fig. 3). The lifetimes of sub-RPE deposits as well as that of the RPE were significantly longer in the AMD eyes compared with sub-RPE deposits and RPE in control eyes (Table 2).

Investigative Ophthalmology & Visual Science

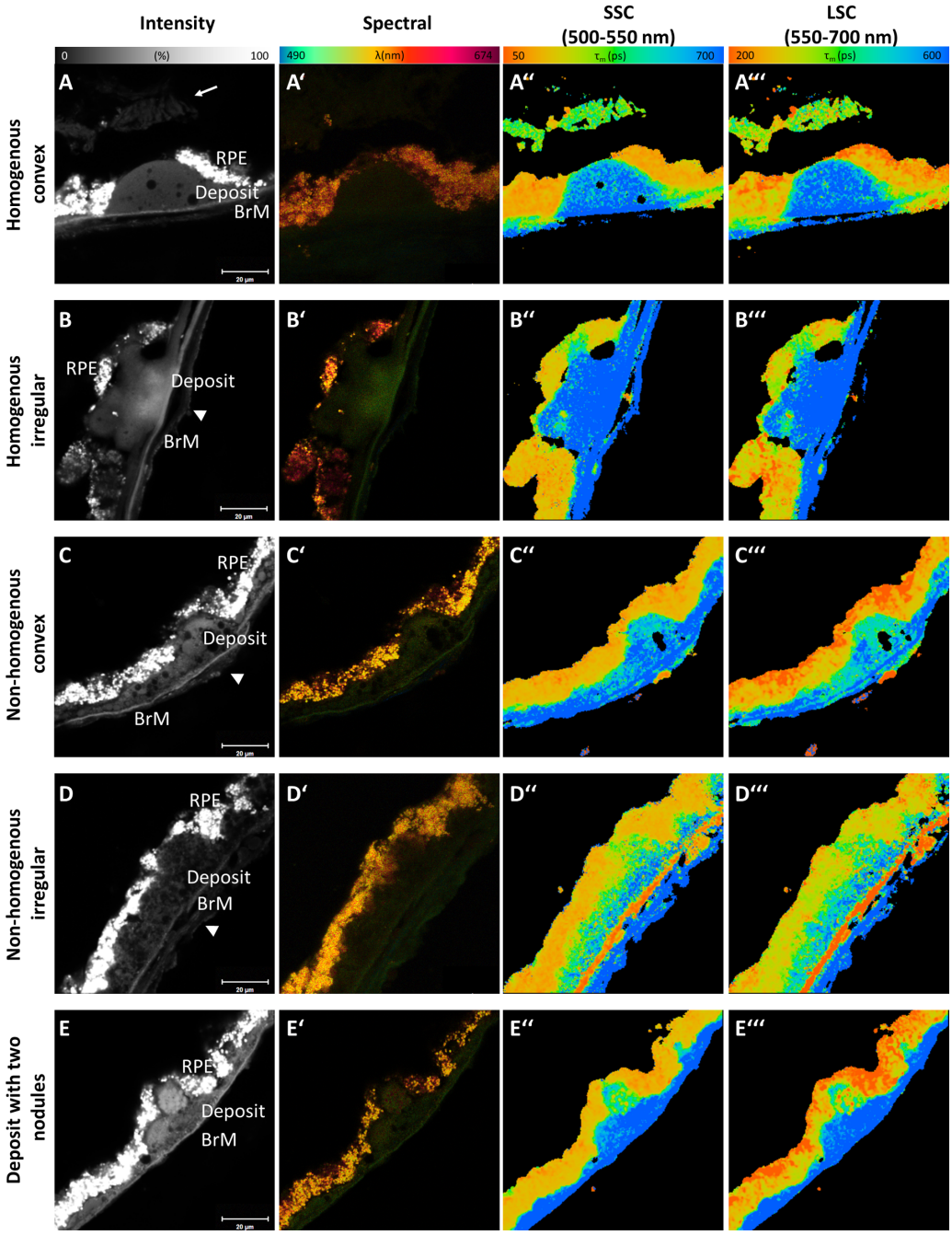

Figure 2. Examples of different sub-RPE deposit types, (**A**) homogenous convex, (**B**) homogenous irregular, partially hyperfluorescent, (**C**) nonhomogenous convex, (**D**) nonhomogenous irregular, (**E**) sub-RPE deposit with two hyperfluorescent nodules (nonhomogenous irregular), Intensity image, autofluorescence emission spectra image and fluorescence lifetimes (τ_m) in SSC and LSC (pseudo-colored), Scale bar = 20 µm, arrow = retina (disrupted preparation artifact), arrowhead = choroid (disrupted preparation artifact).

Homogeneous sub-RPE deposits are more abundant in AMD donors (AMD, 56/76 sub-RPE deposits [73.7%]; control, 19/120 sub-RPE deposits [15.8%]). They had longer lifetimes compared with nonhomogenous sub-RPE deposits in general (SSC, 657 ± 174 ps vs. 534 ± 138 ps; LSC, 605 ± 136 ps vs. 502 ± 100 ps; $P < 0.001$ for both). Especially in AMD donors, homogenous sub-RPE deposits had significantly longer lifetimes compared with the nonhomogenous ones. This finding, however, did not hold for the control subjects (results of subgroup comparisons are listed in Table 3). The shape of the sub-RPE deposits was not differently distributed in AMD and control subjects and had no influence on the lifetimes (data not shown).

As mentioned elsewhere in this article, we differentiated two size ranges of sub-RPE deposits according to clinical diagnostics. Larger sub-RPE deposits had significantly longer lifetimes than the small ones (SSC, 662 ± 171 ps vs. 548 ± 149 ps; LSC, 600 ± 128 ps vs. 518 ± 116 ps; $P < 0.001$ for both).

Investigative Ophthalmology & Visual Science

Table 3. Mean Fluorescence Lifetimes (τ_m) for Homogenous and Nonhomogenous Sub-RPE Deposits (According to Their Appearance in Intensity Images)

	Control	AMD	*P* Value
Homogenous sub-RPE deposits SSC	555 ± 160	691 ± 165	0.003
Homogenous sub-RPE deposits LSC	533 ± 145	629 ± 125	0.007
Nonhomogenous sub-RPE deposits SSC	533 ± 143	535 ± 111	0.959
Nonhomogenous sub-RPE deposits LSC	499 ± 103	517 ± 78	0.473

Values are mean ± standard deviation. Control $n = 19$ for homogenous and 101 for nonhomogenous sub-RPE deposits; AMD $n = 56$ for homogenous and 20 for nonhomogenous sub-RPE deposits, results for the short- (SSC) and long-wavelength spectral channel (LSC) are given, statistic by unpaired Student *t* test.

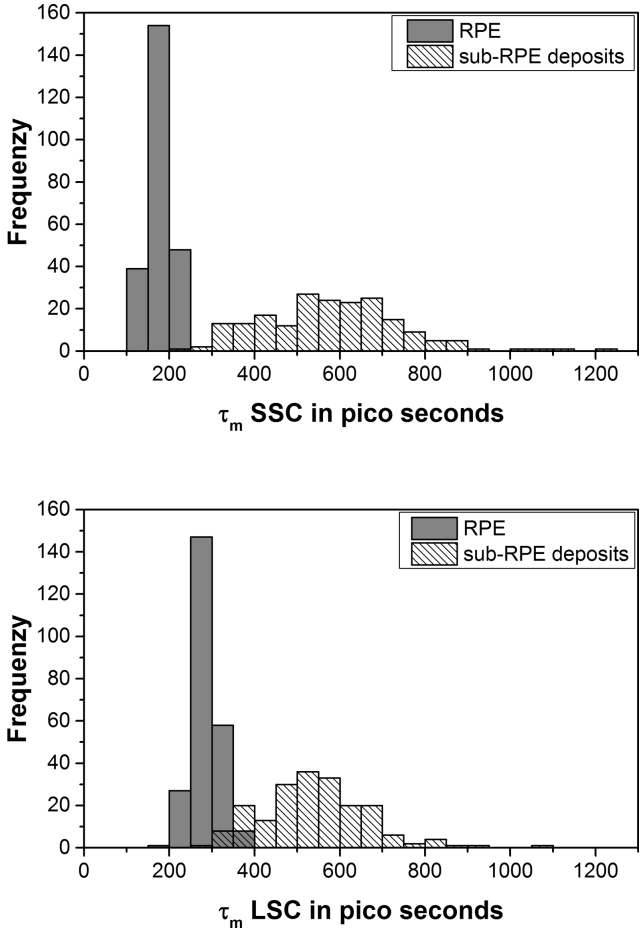

Figure 3. Histograms of mean fluorescence lifetimes (τ_m) for RPE and sub-RPE-deposits. (**Top**) SSC. (**Bottom**) LSC.

Autofluorescence Emission Intensity and Spectra

Averaged spectra are shown in Figure 4. No difference was found between the spectra of fixed and fresh-frozen tissue (data not shown). Therefore, spectra from both preparations were pooled.

The averaged intensity for RPE was 121 ± 3 arbitrary units, and for sub-RPE deposits 26 ± 14 arbitrary units. The intensity of the RPE was on average 6.3 ± 0.3 times higher than for sub-RPE deposits. No deposit was more intense than RPE (Fig. 5). No correlations between RPE and sub-RPE deposits intensity or sub-RPE deposits intensity and lifetime were found.

The fluorescence emission of sub-RPE deposits occurred at a shorter wavelength than that of RPE. The RPE autofluorescence peaks at 610 nm, the peak of sub-RPE deposit autofluorescence was found at 570 nm (Fig. 4A). This difference between RPE and sub-RPE deposits spectra was significant. We found an interaction of category (sub-RPE deposits or RPE) and spectra ($P < 0.001$) as well as category and spectra squared ($P < 0.001$) in the polynomial mixed regression model. The RPE spectra were significantly different for AMD donor eyes and controls ($P = 0.034$ for the interaction between diagnosis [AMD or control] and RPE spectra squared). A slight shift of the rising edge (between 500 and 600 nm) toward shorter wavelengths was observed for AMD donors (Fig. 4C). The same holds for the sub-RPE deposits spectra. Figure 4D shows a slight hypsochromic shift for the AMD donors; the peak was at 570 nm for both groups and the spectra were significantly different ($P = 0.023$ for the interaction between diagnosis and sub-RPE deposits spectra squared). The comparison of sub-RPE deposits of greater than 63 µm with smaller ones showed a slight hypsochromic shift of the larger sub-RPE deposits, but no significant difference (Fig. 4B).

Discussion

Clinical FAF, excited at 488 nm, is thought to originate from lipofuscin and melanolipofuscin in RPE cells.[15–17] In our investigation, as in prior studies,[10] we found histologic autofluorescence also from Bruch's membrane and sub-RPE deposits, such as basal laminar deposits, as well as basal linear deposits and drusen; however, the RPE autofluorescence was by far the strongest. Furthermore, RPE autofluorescence clearly showed the granular structure, known from previous investigations with two-photon[18,19] as well as super-resolution microscopy,[20] and autofluorescence spectrum similarly reported for lipofuscin and melanolipofuscin.[11,21] We found the peak of the RPE spectrum at 610 nm, as was reported by Delori et al.[15] for human post mortem RPE excited at 510 nm. In vivo, these authors found peak emissions at 631 and 621 nm upon 510 and 470 nm excitation, respectively. Thus, slight differences in the emission peak might be due to the excitation conditions (wavelength and 960 nm two-photon excitation vs. one-photon excitation). A dependence of the peak emission on the excitation wavelength was also found by Marmorstein et al.[10] on histology. These authors measured slightly shorter emission peaks for 488 nm excitation (approximately corresponding with our 960 nm two-photon excitation), which might be due to the fact that they used macular samples exclusively. Also, Delori et al.[15] reported shorter emission peaks for the macula than measured at an eccentricity of 7° upon 470 nm excitation in vivo. In contrast, Ben Ami et al.[21] did not find differences in the spectral signature of foveal, perifovea, and near-periphery histologic RPE. For areas of drusen in

Investigative Ophthalmology & Visual Science

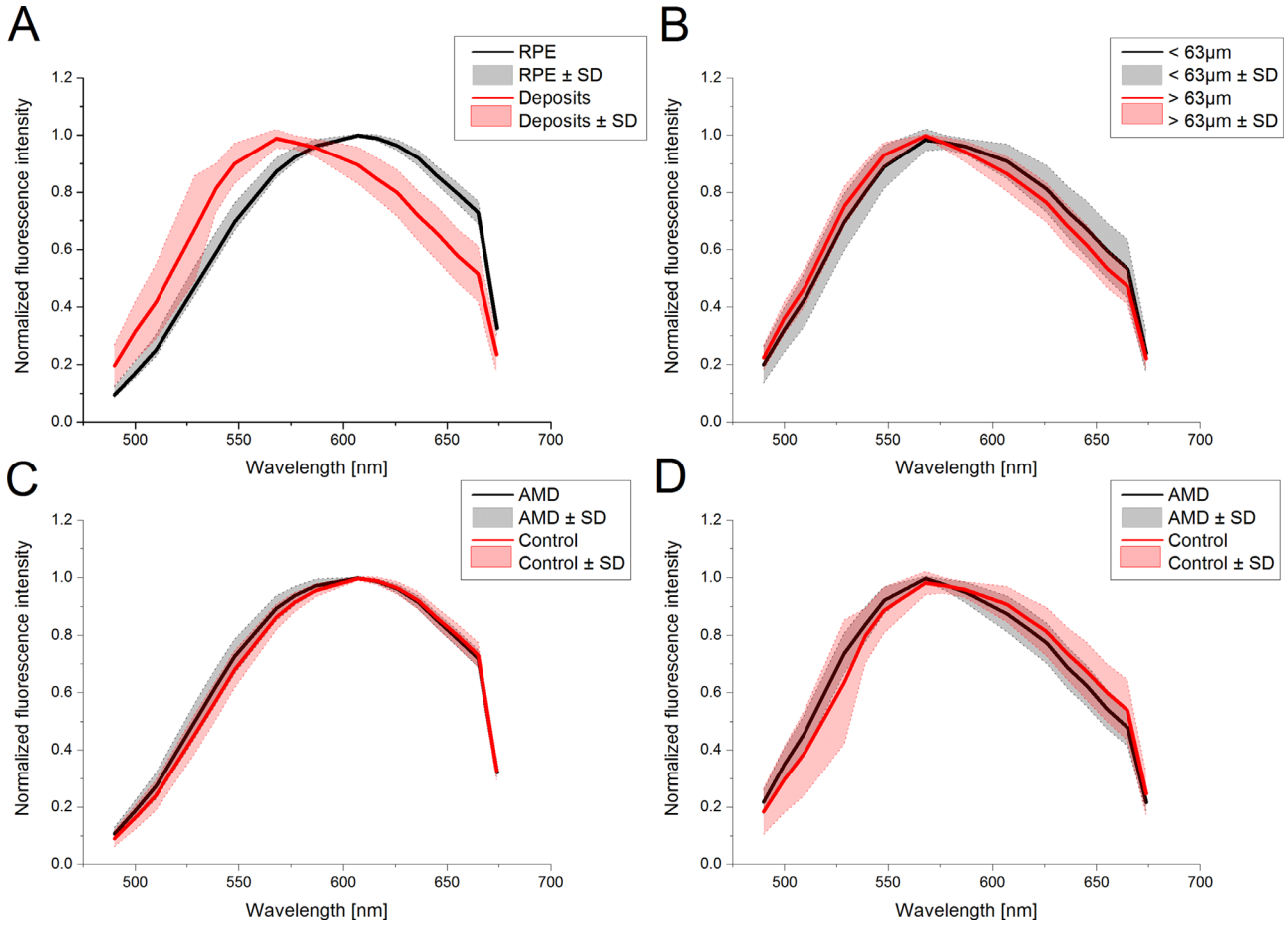

Figure 4. Autofluorescence emission spectra averaged over groups of measurements, filled areas indicate the range of standard deviation. (**A**) Spectra of all sub-RPE deposits (*red*) and RPE (*black*). (**B**) Sub-RPE deposits less than 63 µm (*black*) and greater than 63 µm (*red*) in diameter. (**C**) RPE of AMD donors (*black*) and controls (*red*). (**D**) Sub-RPE deposits of AMD donors (*black*) and controls (*red*).

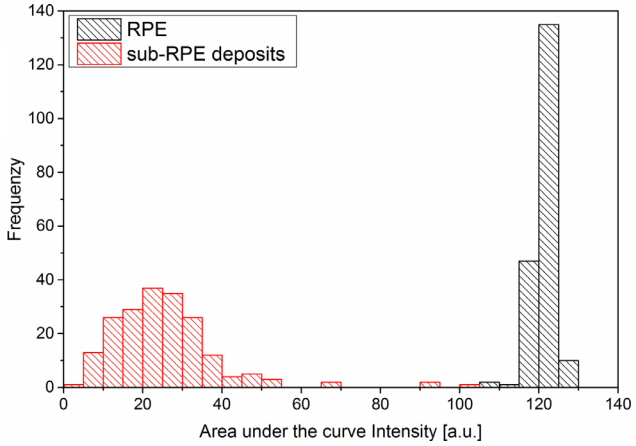

Figure 5. Histogram of RPE and sub-RPE deposit autofluorescence intensities distribution. Intensity is given in arbitrary units (a.u.) and was calculated as area under the curve per ROI.

vivo, Arend et al.[21] found a hypsochromic spectral shift. They revealed a spectrum peaking at 560 nm, which they attributed to drusen autofluorescence. We measured very similar autofluorescence with a peak at 570 nm. Tong et al.[21] reported a drusen-specific spectrum with a peak most abundantly found at 520 nm (excitation 480 nm). This finding is shorter than what we measured. However, we used histologic cross-sections, whereas Tong et al.[21] applied en face imaging, which could yield in autofluorescence contribution also of Bruch's membrane, which is known to have short-wavelength autofluorescence.

Our fluorescence maximum of sub-RPE deposits was 40 nm shorter than that of RPE, which is in agreement with our recent in vivo findings using the two spectral channels of FLIO[6] and indicates that drusen contain other fluorophores than lipofuscin. Although lipofuscin-like inclusions in drusen may occur occasionally, their number is very small[23–25] and should not have a measurable impact on the total drusen autofluorescence. We found slightly hypsochromic shifted spectra of RPE and sub-RPE deposits in AMD donors, compared with controls, as well as of deposits larger than 63 µm in diameter vs. smaller ones upon unchanged peak emission wavelengths. Although the difference of average spectra from AMD and control eyes was significant, it was small (Figs. 4C, 4D) and its diagnostic relevance remains to be determined.

Fluorescence lifetime, however, seems to have high potential for diagnosis. The fluorescence lifetime of the RPE in our study was significantly longer in AMD donor eyes in both spectral channels. This finding was in agreement

Investigative Ophthalmology & Visual Science

with the finding of prolonged fluorescence lifetimes in AMD patients in vivo.[4] The in vivo lifetimes reported in that paper (ocular fundus/RPE in control SSC, 313 ± 79 ps, LSC, 342 ± 124 ps; and in AMD SSC, 340 ± 71 ps, LSC 403 ± 98 ps) are to some extent longer in general compared with our ex vivo findings presented here. This difference might have several reasons. First, although our measurements were close to the in vivo data, we cannot exclude post mortem changes or alterations by the preparation procedure. Second, the in vivo data, recorded from en face images, certainly contain fluorescent components from other tissues than RPE, which might have longer lifetimes. Third, fluorescence excitation by different lasers (femtosecond laser for two-photon excitation in our measurement vs. one-photon excitation with a picosecond laser in vivo), might make a difference.

Drusen are the major intraocular risk factor for progression to advanced AMD (neovascularization or atrophy)[26–28] and may be predictive for the disease progression.[21–23] Several studies investigated the autofluorescence of fundus areas with drusen. We found a very consistent RPE autofluorescence intensity, whereas sub-RPE deposits showed highly diverse intensities, none of which was higher than RPE autofluorescence. For in vivo en face imaging, Delori et al.[29] found hypoautofluorescence of the drusen center, often surrounded by a hyperfluorescent annulus. Göbel et al.[30] found drusen with increased, decreased, as well as unremarkable autofluorescence intensity. In a recent clinical study, we found one-third of soft drusen to be hyperfluorescent.[6] Investigating refractile drusen, Suzuki et al.[31] found a transition from uniform hyper-FAF to a ring of hyper-FAF. Delori et al.[29] explained the central hypofluorescence of drusen with a hyperfluorescent annulus by the thinning of the RPE on top of the druse with a translocation to its rim. It is also possible that photoreceptor shortening on top of the druse contributes to this distinctive appearance.[32,33] Although the drusen autofluorescence, in general, is weaker than that of the RPE, its contribution to the total FAF in in vivo en face imaging can be considerable, if the drusen are much thicker than the RPE, which is a cellular monolayer. FLIO has revealed a wide variety in drusen autofluorescence lifetimes.[3,4,6] Longer fluorescence lifetimes in some of the drusen[4,6] and a general shift toward shorter emission wavelengths compared with the adjacent fundus,[6] however, indicate an independent autofluorescence contribution from the drusen themselves.

To distinguish fluorescence emissions from different fundus layers, in this study we investigated histologic cross-sections. This strategy clearly revealed different fluorescence properties of RPE and drusen. Although drusen can virtually be nonfluorescent, most of them emit fluorescence at shorter wavelength and with longer decay times than the RPE. Thus far, this study confirms in vivo FLIO results[6] and an earlier investigation performing spectrally resolved FLIM in the histology of one AMD and one control donor eye.[12] Relative to our previous study,[12] in histologic cross-sections sub-REP deposit autofluorescence is not overlaid by that of the RPE, and we had more donor material. First, we grouped sub-RPE deposits by their size for comparison of fluorescence parameters. According to clinical AMD classification criteria,[27,34] we distinguished sub-RPE deposits of less than 63 µm which were clearly localized and round, from larger more widespread sub-RPE deposits. The latter, more extended deposits showed significantly longer fluorescence lifetimes, indicating a different fluorophore composition. This difference was clearly underlined by finding some drusen containing two hyperfluorescent nodules (Fig. 2E) with clearly distinct lifetimes. In contrast, longer lifetimes in the larger sub-RPE deposits seem to contradict our in vivo findings, where we observed no difference in large (soft) drusen compared with their surrounding fundus.[6] However, it has to be kept in mind that this holds for hyperfluorescent drusen in vivo only. Also here we found highly fluorescent sub-RPE deposits (Fig. 2B) having long lifetimes, but a general correlation between intensity and lifetimes was not found. Furthermore, a comparison with the in vivo autofluorescence is difficult for small drusen (<63 µm) because these drusen are on the resolution limit of clinical FLIO.

Besides difference in the shape of the sub-RPE deposits (round or stretched at Bruch's membrane, in our study not associated with AMD) and all heterogeneity in fluorescence lifetime, deposits lifetime was significantly longer in donors with AMD than in aged donors lacking clear AMD pathology. Furthermore, the abundance of deposits, especially homogenous ones, was higher in the AMD eyes and the percentage of sub-RPE deposits larger than 63 µm was higher than in the controls. In optical coherence tomography, the most common pattern observed for drusen in eyes of AMD patients was a convex shape with a homogeneous filling.[35] In histology, drusen also significantly differ with respect to their ultrastructural morphology and clear differentiation between homogenous structures and highly heterogeneous ones are possible.[25,36] Soft drusen are described to be made of homogeneous content[25] and have been reported to highly correlated with AMD and AMD progression.[9] One could speculate that the homogenous sub-RPE deposits with long lifetimes, found in AMD patients, are soft drusen. Our findings underscore that drusen are linked to AMD pathology. However, the higher lifetime of deposits in AMD also indicates that a different composition might hint to the disease.

Drusen and basal linear deposits are extracellular accumulations of lipids, phospholipids, (lipo-)proteins, and minerals. Plasma LDL and HDL deliver essential lipophilic compounds such as vitamins A and E, lutein, and cholesterol to the RPE and outer retina.[37–39] Furthermore, apoA, B, and E lipoproteins, secreted from the RPE, may bind to Bruch's membrane.[40,41] Subsequently, those lipoproteins may degrade and fuse to a lipid pool, according to Curcio et al.,[9,42] analogous to an oil spill. Unfortunately, little is known about the autofluorescence of such lipids upon blue light or two-photon infrared (IR) excitation, respectively. However, because drusen formation shares some similarity with that of atherosclerotic plaques,[9] where blood LDL binds to the extracellular matrix of the vessel wall,[43,44] a comparison with fluorescence investigations in those plaques is interesting.[45] Even though the majority of plasma lipids are nonfluorescent,[46,47] the lipid core of LDL-containing atherosclerotic plaques emits red fluorescence with peak intensity at 500 nm upon excitation at 350 nm. The core contains cholesteryl esters and oxidative products of phospholipids, such as lysophosphatidylcholine.[48] Park et al.[49] found an emission at 550 nm from the lipids in the plaques, which was distinguishable from the autofluorescence of collagen (λ_{em} of 370–450 nm) and elastin (λ_{em} of 360–500 nm). This lipid fluorescence showed a long lifetime of 5.3 ns. This lifetime is considerably longer than the one we measured for sub-RPE deposits. That could be due to different instrumentation and fluorescence excitation conditions (Park et al. used a Nd:YAG laser, 355 nm/1 ns). In contrast, drusen might be more complex than atherosclerotic plaques because not only serum-derived lipids contribute

to their formation, but also molecules from photoreceptor degradation as well as visual pigment turnover forming lipoprotein-derived and retinaldehyde adducts-containing debris.[9,42]

Several limitations of this study have to be mentioned. There were no clinical data or diagnosis available for the donor eyes. Thus, classification in AMD or control had to rely on post mortem fundus inspection and optical coherence tomography plus histology. Furthermore, only small and intermediate sub-RPE deposits were found in the samples. However, it cannot be excluded that larger soft drusen were present initially, but were lost in the tissue preparation and slicing procedure because soft drusen are biomechanically fragile. In addition, it was not always possible to separate drusen and basal linear deposits autofluorescence from that of basal laminar deposits.

The measured sub-RPE deposits size might have been underestimated owing to off-axis cuts that missed the largest part of the deposit. However, despite this systematic underestimation of the sub-RPE deposits size, a significant difference of fluorescence lifetimes for deposits, measured smaller or larger than 63 µm, was found, and this finding has to be considered as a matter of fact. This study used two-photon excitation of the fluorescence because this gives a better spatial resolution, especially of the FLIM images recorded by detectors at the nondescanned port of the microscope. This feature, however, limits somewhat the comparability with in vivo FLIO measurements, which use one-photon picosecond fluorescence excitation. Nevertheless, in this study we found similar lifetimes as in vivo. Although fixation, in agreement with Delori et al.,[15] seems to have only minor impact on fluorescence spectra as well as lifetimes, it has to be pointed out that post mortem changes of fluorophore composition and properties of the embedding matrix may have occurred. Additionally, preparation of the donor eyes for cryosectioning may alter fluorescence lifetimes by a change of the viscosity of the sample while they are frozen. These factors all limit the comparability of our results with in vivo findings. However, the lifetimes, found for RPE, are similar to those reported from in vivo studies. Thus, we assume that also the prolongation as well as the diversity of sub-RPE deposit fluorescence lifetimes reflects the in vivo situation at least qualitatively.

Taken together, we found considerably longer fluorescence lifetimes for sub-RPE deposits than for RPE. Furthermore, the lifetime was longer for larger deposits and deposits with homogenous autofluorescence patterns. The lifetime of deposits as well as RPE was longer in AMD eyes than in controls. Deposits emitted autofluorescence at shorter wavelengths than RPE and showed a slight hypsochromic shift in AMD eyes. The clearer differences for sub-RPE depositions in lifetime measurements compared with the spectra make lifetime measurements a great enrichment for autofluorescence studies, provides more insight into the composition of sub-RPE depositions, and might help to differentiate changes associated with AMD development in future studies.

Acknowledgments

Supported by NIH grant 1R01EY027948.

Disclosure: **R. Schultz,** None; **K.C.L.K. Gamage,** None; **J.D. Messinger,** None; **C.A. Curcio,** None; **M. Hammer,** None

References

1. Bindewald A, Bird AC, Dandekar SS, et al. Classification of fundus autofluorescence patterns in early age-related macular disease. *Invest Ophthalmol Vis Sci*. 2005;46:3309–3314.
2. Einbock W, Moessner A, Schnurrbusch UE, Holz FG, Wolf S. Changes in fundus autofluorescence in patients with age-related maculopathy. Correlation to visual function: a prospective study. *Graefes Arch Clin Exp Ophthalmol*. 2005;243:300–305.
3. Dysli C, Fink R, Wolf S, Zinkernagel MS. Fluorescence lifetimes of drusen in age-related macular degeneration. *Invest Ophthalmol Vis Sci*. 2017;58:4856–4862.
4. Sauer L, Gensure RH, Andersen KM, et al. Patterns of fundus autofluorescence lifetimes in eyes of individuals with nonexudative age-related macular degeneration. *Invest Ophthalmol Vis Sci*. 2018;59:AMD65–AMD77.
5. Sauer L, Komanski CB, Vitale AS, Hansen ED, Bernstein PS. Fluorescence lifetime imaging ophthalmoscopy (FLIO) in eyes with pigment epithelial detachments due to age-related macular degeneration. *Invest Ophthalmol Vis Sci*. 2019;60:3054–3063.
6. Hammer M, Schultz R, Hasan S, et al. Fundus autofluorescence lifetimes and spectral features of soft drusen and hyperpigmentation in age-related macular degeneration. *Transl Vis Sci Technol*. 2020;9:20.
7. Katz ML, Eldred GE, Robison WG. Lipofuscin autofluorescence - evidence for vitamin-A involvement in the retina. *Mech Ageing Dev*. 1987;39:81.
8. Sparrow JR, Yoon KD, Wu Y, Yamamoto K. Interpretations of fundus autofluorescence from studies of the bisretinoids of the retina. *Invest Ophthalmol Vis Sci*. 2010;51:4351–4357.
9. Curcio CA. Soft drusen in age-related macular degeneration: biology and targeting via the oil spill strategies. *Invest Ophthalmol Vis Sci*. 2018;59:AMD160–AMD181.
10. Marmorstein AD, Marmorstein LY, Sakaguchi H, Hollyfield JG. Spectral profiling of autofluorescence associated with lipofuscin, Bruch's membrane, and sub-RPE deposits in normal and AMD eyes. *Invest Ophthalmol Vis Sci*. 2002;43:2435–2441.
11. Tong Y, Ben Ami T, Hong S, et al. Hyperspectral autofluorescence imaging of drusen and retinal pigment epithelium in donor eyes with age-related macular degeneration. *Retina*. 2016;36(Suppl 1):S127–S136.
12. Schweitzer D, Gaillard ER, Dillon J, et al. Time-resolved autofluorescence imaging of human donor retina tissue from donors with significant extramacular drusen. *Invest Ophthalmol Vis Sci*. 2012;53:3376–3386.
13. Anderson DMG, Messinger JD, Patterson NH, et al. Lipid landscape of the human retina and supporting tissues revealed by high resolution imaging mass spectrometry. *J Am Soc Mass Spectrom*. 2020.
14. Becker W. Fluorescence lifetime imaging–techniques and applications. *J Microsc*. 2012;247:119–136.
15. Delori FC, Dorey KC, Staurenghi G, Arend O, Goger DC, Weiter JJ. In vivo fluorescence of the ocular fundus exhibits retinal pigment epithelium lipofuscin characteristics. *Invest Ophthalmol*. 1995;36:718–729.
16. von Rückmann A, Fitzke FW, Bird AC. Fundus autofluorescence in age-related macular disease imaged with a laser scanning ophthalmoscope. *Invest Ophthalmol Vis Sci*. 1997;38:478–486.
17. Holz FG, Bellman C, Staudt S, Schutt F, Volcker HE. Fundus autofluorescence and development of geographic atrophy in age- related macular degeneration. *Invest Ophthalmol Vis Sci*. 2001;42:1051–1056.
18. Bindewald-Wittich A, Han M, Schmitz-Valckenberg S, et al. Two-photon-excited fluorescence imaging of human RPE

Investigative Ophthalmology & Visual Science

cells with a femtosecond Ti:Sapphire laser. *Invest Ophthalmol Vis Sci*. 2006;47:4553–4557.

19. Han M, Bindewald-Wittich A, Holz FG, et al. Two-photon excited autofluorescence imaging of human retinal pigment epithelial cells. *J Biomed Opt*. 2006;11:010501.
20. Ach T, Tolstik E, Messinger JD, Zarubina AV, Heintzmann R, Curcio CA. Lipofuscin redistribution and loss accompanied by cytoskeletal stress in retinal pigment epithelium of eyes with age-related macular degeneration. *Invest Ophthalmol Vis Sci*. 2015;56:3242–3252.
21. Ben Ami T, Tong Y, Bhuiyan A, et al. Spatial and spectral characterization of human retinal pigment epithelium fluorophore families by ex vivo hyperspectral autofluorescence imaging. *Transl Vis Sci Technol*. 2016;5:5.
22. Arend O, Weiter JJ, Goger DG, Delori FC. In vivo Fundus Fluoreszenzmessungen bei Patienten mit altersbedingtrer Makuladegeneration. *Der Ophthalmologe*. 1995;92:647–653.
23. Anderson DH, Ozaki S, Nealon M, et al. Local cellular sources of apolipoprotein E in the human retina and retinal pigmented epithelium: implications for the process of drusen formation. *Am J Ophthalmol*. 2001;131:767–781.
24. Rossberger S, Ach T, Best G, Cremer C, Heintzmann R, Dithmar S. High-resolution imaging of autofluorescent particles within drusen using structured illumination microscopy. *Br J Ophthalmol*. 2013;97:518–523.
25. Rudolf M, Clark ME, Chimento MF, Li CM, Medeiros NE, Curcio CA. Prevalence and morphology of druse types in the macula and periphery of eyes with age-related maculopathy. *Invest Ophthalmol Vis Sci*. 2008;49:1200–1209.
26. Klein R, Klein BE, Knudtson MD, Meuer SM, Swift M, Gangnon RE. Fifteen-year cumulative incidence of age-related macular degeneration: the Beaver Dam Eye Study. *Ophthalmology*. 2007;114:253–262.
27. Klaver CC, Assink JJ, van Leeuwen R, et al. Incidence and progression rates of age-related maculopathy: the Rotterdam Study. *Invest Ophthalmol Vis Sci*. 2001;42:2237–2241.
28. Wang JJ, Rochtchina E, Lee AJ, et al. Ten-year incidence and progression of age-related maculopathy: the blue Mountains Eye Study. *Ophthalmology*. 2007;114:92–98.
29. Delori FC, Fleckner MR, Goger DG, Weiter JJ, Dorey CK. Autofluorescence distribution associated with drusen in age-related macular degeneration. *Invest Ophthalmol Vis Sci*. 2000;41:496–504.
30. Gobel AP, Fleckenstein M, Heeren TF, Holz FG, Schmitz-Valckenberg S. In-vivo mapping of drusen by fundus autofluorescence and spectral-domain optical coherence tomography imaging. *Graefes Arch Clin Exp Ophthalmol*. 2016;254:59–67.
31. Suzuki M, Curcio CA, Mullins RF, Spaide RF. Refractile drusen: clinical imaging and candidate histology. *Retina*. 2015;35:859–865.
32. Theelen T, Berendschot TT, Boon CJ, Hoyng CB, Klevering BJ. Analysis of visual pigment by fundus autofluorescence. *Exp Eye Res*. 2008;86:296–304.
33. Freund KB, Mrejen S, Jung J, Yannuzzi LA, Boon CJ. Increased fundus autofluorescence related to outer retinal disruption. *JAMA Ophthalmol*. 2013;131:1645–1649.
34. AREDS Study Group. The age-related eye disease study system for classifying age-related macular degeneration from stereoscopic color fundus photographs: the age-related eye disease study report number 6. *Am J Ophthalmol*. 2001;132:668–681.
35. Khanifar AA, Koreishi AF, Izatt JA, Toth CA. Drusen ultrastructure imaging with spectral domain optical coherence tomography in age-related macular degeneration. *Ophthalmology*. 2008;115:1883–1890.
36. Hageman GS, Mullins RF. Molecular composition of drusen as related to substructural phenotype. *Mol Vis*. 1999;5:28.
37. Farkas TG, Sylvester V, Archer D, Altona M. The histochemistry of drusen. *Am J Ophthalmol*. 1971;71:1206–1215.
38. Sarks SH. Council Lecture. Drusen and their relationship to senile macular degeneration. *Aust J Ophthalmol*. 1980;8:117–130.
39. Pauleikhoff D, Zuels S, Sheraidah GS, Marshall J, Wessing A, Bird AC. Correlation between biochemical composition and fluorescein binding of deposits in Bruch's membrane. *Ophthalmology*. 1992;99:1548–1553.
40. Curcio CA, Millican CL, Bailey T, Kruth HS. Accumulation of cholesterol with age in human Bruch's membrane. *Invest Ophthalmol Vis Sci*. 2001;42:265–274.
41. Wang L, Li CM, Rudolf M, et al. Lipoprotein particles of intraocular origin in human Bruch membrane: an unusual lipid profile. *Invest Ophthalmol Vis Sci*. 2009;50:870–877.
42. Curcio CA, Johnson M, Rudolf M, Huang J-D. The oil spill in ageing Bruch membrane. *Br J Ophthalmol*. 2011;95:1638–1645.
43. Guyton JR, Klemp KF. The lipid-rich core region of human atherosclerotic fibrous plaques. Prevalence of small lipid droplets and vesicles by electron microscopy. *Am J Pathol*. 1989;134:705–717.
44. Guyton JR, Klemp KF. Transitional features in human atherosclerosis. Intimal thickening, cholesterol clefts, and cell loss in human aortic fatty streaks. *Am J Pathol*. 1993;143:1444–1457.
45. Bocan TM, Guyton JR. Human aortic fibrolipid lesions. Progenitor lesions for fibrous plaques, exhibiting early formation of the cholesterol-rich core. *Am J Pathol*. 1985;120:193–206.
46. Uchida Y, Uchida Y, Kawai S, et al. Detection of vulnerable coronary plaques by color fluorescent angioscopy. *JACC Cardiovasc Imaging*. 2010;3:398–408.
47. Uchida Y, Maezawa Y, Uchida Y, Hiruta N, Shimoyama E. Molecular imaging of low-density lipoprotein in human coronary plaques by color fluorescent angioscopy and microscopy. *PLoS One*. 2012;7:e50678.
48. Arakawa K, Isoda K, Ito T, Nakajima K, Shibuya T, Ohsuzu F. Fluorescence analysis of biochemical constituents identifies atherosclerotic plaque with a thin fibrous cap. *Arterioscler Thromb Vasc Biol*. 2002;22:1002–1007.
49. Park J, Pande P, Shrestha S, Clubb F, Applegate BE, Jo JA. Biochemical characterization of atherosclerotic plaques by endogenous multispectral fluorescence lifetime imaging microscopy. *Atherosclerosis*. 2012;220:394–401.

Investigative Ophthalmology & Visual Science